The Second Data Release of the Survey of the MAgellanic Stellar History (SMASH)

David Nidever, Knut Olsen, Yumi Choi, Tomas Ruiz-Lara, Amy Miller, L. Clifton Johnson, Cameron Bell, Robert Blum, Maria-Rosa Cioni, Carme Gallart, et al.

The Astronomical Journal, 161:74 (13pp), 2021 February https://doi.org/10.3847/1538-3881/abceb7

The Second Data Release of the Survey of the MAgellanic Stellar History (SMASH)

David L. Nidever[1,2], Knut Olsen[2], Yumi Choi[1,3,4], Tomas Ruiz-Lara[5,6,7], Amy E. Miller[1,8], L. Clifton Johnson[9], Cameron P. M. Bell[8], Robert D. Blum[10], Maria-Rosa L. Cioni[8], Carme Gallart[6,7], Steven R. Majewski[11], Nicolas F. Martin[12,13], Pol Massana[14], Antonela Monachesi[15,16], Noelia E. D. Noël[14], Joanna D. Sakowska[14], Roeland P. van der Marel[3,17], Alistair R. Walker[18], Dennis Zaritsky[4], Eric F. Bell[19], Blair C. Conn[20,21], Thomas J. L. de Boer[22], Robert A. Gruendl[23,24], Matteo Monelli[6,7], Ricardo R. Muñoz[25], Abhijit Saha[2], A. Katherina Vivas[18], Edouard Bernard[26], Gurtina Besla[4], Julio A. Carballo-Bello[27], Antonio Dorta[6,7], David Martinez-Delgado[28], Alex Goater[14], Vadim Rusakov[29,30], and Guy S. Stringfellow[31]

[1] Department of Physics, Montana State University, P.O. Box 173840, Bozeman, MT 59717-3840, USA; dnidever@montana.edu
[2] NSF's National Optical-Infrared Astronomy Research Laboratory, 950 North Cherry Avenue, Tucson, AZ 85719, USA
[3] Space Telescope Science Institute, 3700 San Martin Drive, Baltimore, MD 21218, USA
[4] Steward Observatory, University of Arizona, 933 North Cherry Avenue, Tucson, AZ 85721, USA
[5] Kapteyn Astronomical Institute, University of Groningen, Landleven 12, 9747 AD Groningen, The Netherlands
[6] Instituto de Astrofísica de Canarias, La Laguna, Tenerife, Spain
[7] Departamento de Astrofísica, Universidad de La Laguna, Tenerife, Spain
[8] Leibniz-Institut für Astrophysik Potsdam (AIP), An der Sternwarte 16, D-14482 Potsdam, Germany
[9] Center for Interdisciplinary Exploration and Research in Astrophysics (CIERA) and Department of Physics and Astronomy, Northwestern University, 1800 Sherman Avenue, Evanston, IL 60201, USA
[10] NSF's National Optical-Infrared Astronomy Research Laboratory/LSST, 950 North Cherry Avenue, Tucson, AZ 85719, USA
[11] Department of Astronomy, University of Virginia, Charlottesville, VA 22904, USA
[12] Université de Strasbourg, CNRS, Observatoire astronomique de Strasbourg, UMR 7550, F-67000 Strasbourg, France
[13] Max-Planck-Institut für Astronomie, Königstuhl 17, D-69117 Heidelberg, Germany
[14] Department of Physics, University of Surrey, Guildford, GU2 7XH, UK
[15] Instituto de Investigacin Multidisciplinar en Ciencia y Tecnologa, Universidad de La Serena, Ral Bitrn 1305, La Serena, Chile
[16] Departamento de Astronomía, Universidad de La Serena, Av. Juan Cisternas 1200 Norte, La Serena, Chile
[17] Center for Astrophysical Sciences, Department of Physics & Astronomy, Johns Hopkins University, Baltimore, MD 21218, USA
[18] Cerro Tololo Inter-American Observatory, NSF's National Optical-Infrared Astronomy Research Laboratory, Casilla 603, La Serena, Chile
[19] Department of Astronomy, University of Michigan, 1085 S. University Avenue, Ann Arbor, MI 48109-1107, USA
[20] Research School of Astronomy & Astrophysics, Mount Stromlo Observatory, Cotter Road, Weston Creek, ACT 2611, Australia
[21] Presently: Analytics, IAG Limited, Level 4, Darling Park Tower 2, 201 Sussex Street, Sydney, NSW 2000, Australia
[22] Institute for Astronomy, University of Hawaii, 2680 Woodlawn Drive Honolulu, HI 96822-1897, USA
[23] National Center for Supercomputing Applications, 1205 West Clark Street, Urbana, IL 61801, USA
[24] Department of Astronomy, University of Illinois, 1002 West Green Street, Urbana, IL 61801, USA
[25] Departamento de Astronomía, Universidad de Chile, Camino del Observatorio 1515, Las Condes, Santiago, Chile
[26] Université Côte d'Azur, OCA, CNRS, F-06304, Nice, Lagrange, France
[27] Instituto de Alta Investigación, Universidad de Tarapacá, Casilla 7D, Arica, Chile
[28] Instituto de Astrofísica de Andalucía, CSIC, E-18080, Granada, Spain
[29] Cosmic Dawn Center (DAWN), Denmark
[30] Niels Bohr Institute, University of Copenhagen, Lyngbyvej 2, DK-2100 Copenhagen Ø, Denmark
[31] Center for Astrophysics and Space Astronomy, University of Colorado, 389 UCB, Boulder, CO 80309-0389, USA
Received 2020 September 30; revised 2020 November 26; accepted 2020 November 26; published 2021 January 20

Abstract

The Large and Small Magellanic Clouds (LMC and SMC) are the largest satellite galaxies of the Milky Way and close enough to allow for a detailed exploration of their structure and formation history. The Survey of the MAgellanic Stellar History (SMASH) is a community Dark Energy Camera (DECam) survey of the Magellanic Clouds using ∼50 nights to sample over ∼2400 deg^2 centered on the Clouds at ∼20% filling factor (but with contiguous coverage in the central regions) and to depths of ∼24th mag in *ugriz*. The primary goals of SMASH are to map out the extended stellar peripheries of the Clouds and uncover their complicated interaction and accretion history as well as to derive spatially resolved star formation histories of the central regions and create a "movie" of their past star formation. Here we announce the second SMASH public data release (DR2), which contains all 197 fully calibrated DECam fields including the main body fields in the central regions. The DR2 data are available through the Astro Data Lab hosted by the NSF's National Optical-Infrared Astronomy Research Laboratory. We highlight three science cases that make use of the SMASH DR2 data and will be published in the future: (1) preliminary star formation histories of the LMC, (2) the search for Magellanic star clusters using citizen scientists, and, (3) photometric metallicities of Magellanic Cloud stars using the DECam *u*-band.

Unified Astronomy Thesaurus concepts: Magellanic Clouds (990); Local Group (929); Milky Way Galaxy (1054); Dwarf galaxies (416); Dwarf irregular galaxies (417); Surveys (1671); Large Magellanic Cloud (903); Small Magellanic Cloud (1468); Photometry (1234); CCD photometry (208)

Supporting material: machine-readable table

1. Introduction

The relative proximity (∼55 kpc) of the Large and Small Magellanic Clouds (LMC and SMC)—the largest satellite galaxies of the Milky Way (MW)—presents opportunities to perform detailed resolved studies on their stellar populations and to uncover their structure, evolution, and past interactions. Systems like the Magellanic Clouds (MCs) are rare in the local galactic neighborhood because they are in close proximity to their host, are a binary pair (Besla et al. 2018), and have vigorous ongoing star formation (e.g., Harris & Zaritsky 2004, 2009; Weisz et al. 2013; Meschin et al. 2014; Rubele et al. 2018). Their active star formation is partially due to their large masses ($M_{\rm LMC} = 1.38 \pm 0.24 \times 10^{11}\,M_{\odot}$, Erkal et al. 2019; $M_{\rm SMC} = 2.1 \times 10^{10}\,M_{\odot}$, Besla et al. 2012), which allows them to retain their gas longer, but also due to the fact they are on their first infall into the MW potential (Kallivayalil et al. 2006, 2013; Besla et al. 2007) and have therefore gone largely unscathed from the inhospitable environment close to large galaxies.

The MCs subtend many hundreds of square degrees in the sky, which makes them challenging to study comprehensively. Apart from the photographic plate (de Vaucouleurs 1955a, 1955b; Irwin 1991; Gardiner & Hatzidimitriou 1992) and wide-field CCD works (Bothun & Thompson 1988), most early studies of field MC stars focused on a number of small regions in them, providing the very first color–magnitude diagrams (CMDs) of their bright stars (e.g., Westerlund 1970; Frogel & Blanco 1983; Hardy et al. 1984; Stryker 1984; Hodge 1987; Bertelli et al. 1992). More recently, large ground-based CCD observing campaigns mapped the inner regions of the MCs (Optical Gravitational Lensing Experiment (OGLE), Udalski et al. 1992; Magellanic Clouds Photometric Survey (MCPS), Zaritsky et al. 2002; SuperMACHO, Rest et al. 2005). Deep ground-based observations were able to derive ages for MC and Galactic clusters (e.g., Brocato et al. 1996). Soon thereafter, the Hubble Space Telescope (HST) provided very deep CMDs reaching well below the oldest main-sequence turnoffs (e.g., Elson et al. 1997; Holtzman et al. 1999; Olsen 1999; Smecker-Hane et al. 2002; Cignoni et al. 2013), albeit for very small fields of view in the crowded inner regions. Soon after it was shown that similar quality data could be obtained from the ground for less crowded areas (see Monteagudo et al. 2018 for ground-based CMDs reaching the oldest main-sequence turn off (oMSTO) for the inner disk and bar of the LMC). In this way, the outer disk and periphery of the LMC was explored with island fields by Gallart et al. (2004, 2008), Majewski et al. (2009), and Saha et al. (2010), while the SMC was targeted by Noël & Gallart (2007) and Nidever et al. (2011). Saha et al. (2010) and Majewski et al. (2009) found extended LMC stellar populations out to ∼16°–20° while Nidever et al. (2011) found red giant branch stars out to a radius of 11° in the SMC. In the last decade, the advent of large field-of-view, multi-CCD detectors has greatly enhanced the ability to map the MCs. The VISTA survey of the Magellanic Clouds system (VMC; Cioni et al. 2011) is mapping the main bodies of the MCs in near-infrared bands, while the STEP (The SMC in Time: Evolution of a Prototype interacting late-type dwarf galaxy; Ripepi et al. 2014) and YMCA (Yes, Magellanic Clouds Again; Gatto et al. 2020) surveys are using the VLT Survey Telescope (VST) to map the Magellanic periphery in optical bands. The construction of the Dark Energy Camera (DECam; Flaugher et al. 2015) on the Blanco 4 m telescope at Cerro Tololo Inter-American Observatory (CTIO) has enabled deep and efficient imaging of the whole southern sky in the last seven years. The Dark Energy Survey (DES; Dark Energy Survey Collaboration et al. 2016) mapped ∼5000 square degrees including part of the MCs, using data obtained with DECam. There are two ongoing surveys that also use DECam to study areas around the MCs: (1) the Magellanic Satellites Survey (MagLites; Torrealba et al. 2018), which will map ∼1200 deg^2 near the south celestial pole and (2) the DECam Local Volume Exploration (DELVE; Mau et al. 2020) survey that has an MC component that will map ∼1000 deg^2 of the Magellanic periphery. Both MagLites and DELVE have goals to search for ultra-faint dwarf galaxy satellites near the LMC and SMC.

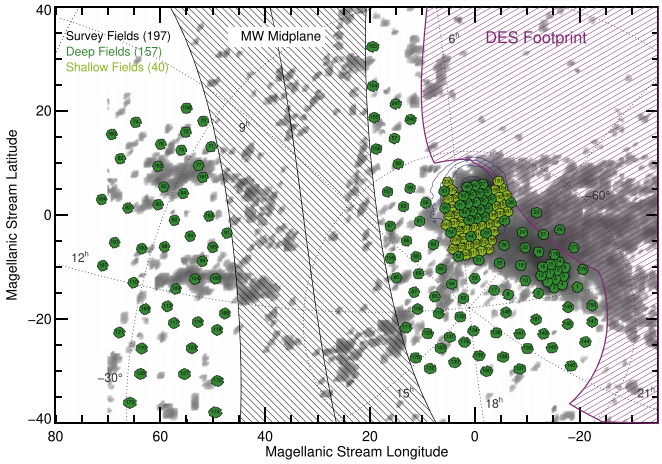

Figure 1. Map of the SMASH survey. The Nidever et al. (2010) observed H I column density of the Magellanic system is shown in the background grayscale. The SMASH fields are shown as filled green hexagons (dark green, deep; light green, shallow). The Milky Way midplane extending to ±15° in latitude is indicated by the black shaded region and was avoided by SMASH. The purple shaded region indicates the DES footprint.

The Survey of the MAgellanic Stellar History (SMASH; Nidever et al. 2017) is a large, community NOAO[32] survey of the MCs using ∼50 nights of DECam time. SMASH maps over 480 square degrees of the sky, contained within ∼2400 square degrees of the Magellanic System (see Figure 1) complementary to the DES coverage. The main goals of SMASH are to (a) search for low surface-brightness structure in the periphery of the MCs, (b) search for the stellar component of the Magellanic Stream and Leading Arm, and (c) derive precise, spatially resolved star formation histories (SFHs) to ancient ages. Nidever et al. (2017) have laid out the survey details (strategy, observations, and data reduction and calibration) and presented the first data release (DR1) of 61 SMASH fields as well as some science examples.

Besides the main goals outlined above, SMASH data have produced many science results. We serendipitously discovered the Hydra II dwarf galaxy (Martin et al. 2015) and used follow-up observations to discover one RR Lyrae star in this satellite (Vivas et al. 2016). A more extensive search for stellar overdensities detected SMASH 1, which appears to be a tidally disrupting globular cluster in the periphery of the LMC (Martin et al. 2016). Choi et al. (2018a) used SMASH data to map the 2D dust reddening and 3D structure of the LMC, confirming previous findings of a stellar warp in the inner disk and discovering a major stellar warp in the outer disk. SMASH also

[32] NOAO is now wholly encompassed in the NSF's National Optical-Infrared Research Laboratory under the programs Mid-scale Observatories (MSO) and Community Science and Data Center. The Kitt Peak National Observatory and Cerro Tololo Inter-American Observatory are both part of MSO.

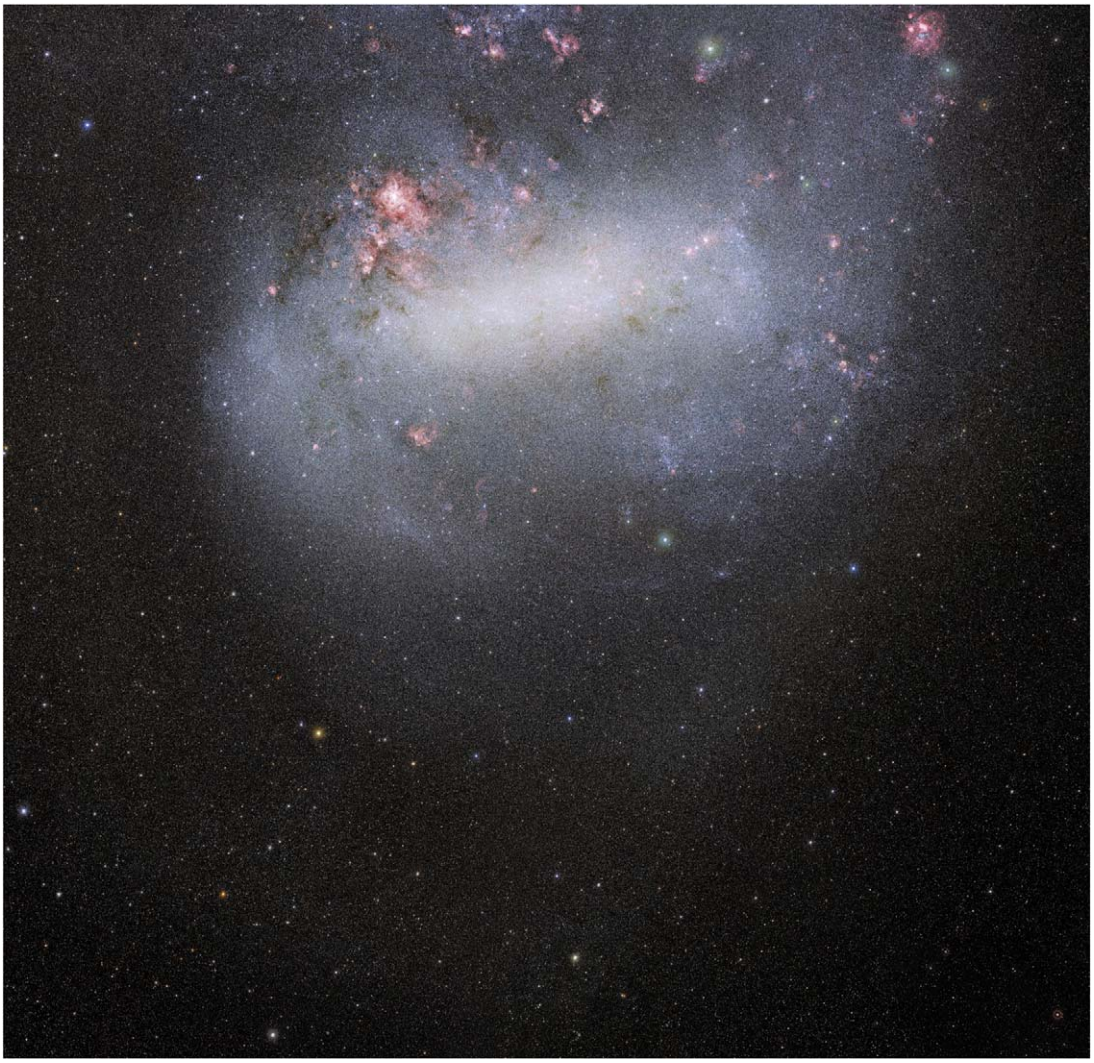

Figure 2. A three-color image of the SMASH fields in the main body of the Large Magellanic Cloud. Credit: CTIO/NOIRLab/NSF/AURA.

demonstrated the existence of a ring-like stellar overdensity in the LMC, which was likely created by recent, close tidal interactions with the SMC (Choi et al. 2018b). Nidever et al. (2019) found evidence of old LMC MSTO stars out to roughly 18.5 kpc from the LMC center, while Massana et al. (2020) detect the disturbed stellar structures in the periphery of the SMC out to ∼8 kpc. Martínez-Delgado et al. (2019) investigated a shell of stars located 1.°9 from the SMC center, and found that it is composed of young stars, suggesting a recent star formation event triggered by a direct collision between the MCs. Bell et al. (2019, 2020) used a combination of SMASH and VMC data to map the total intrinsic extinction through the SMC using spectral energy distributions of background galaxies.

In this paper we describe the second public data release from the SMASH survey, which includes—for the first time—DECam data in the central regions of the MCs (see Figures 2 and 3), and we present preliminary analyses of the science cases that have so far been conducted using SMASH DR2. The layout of this paper is as follows. Section 2 briefly describes our final observations while Section 3 outlines some of the modifications of the data processing compared to DR1. Section 4 describes the data release files and the achieved performance while Section 5 reviews the capabilities available in the Astro Data Lab. Finally, Section 6 presents three science examples using SMASH DR2 data.

2. Observations

Some additional observations were obtained after the release of SMASH DR1 (Nidever et al. 2017). Most of these were using Director's Discretionary (DD) time or Engineering time to obtain short exposures during photometric conditions to calibrate previous data that were obtained in nonphotometric conditions. The list of SMASH fields is available in the machine-readable version of Table 1 and the full list of SMASH observations are summarized in Table 2. The median seeing in the observations is 1.″22 (u), 1.″13 (g), 1.″01 (r), 0.″95 (i), and 0.″90 (z) with a scatter of roughly 0.″25.

3. Data Processing and Calibration

The SMASH data reduction is described in detail in Nidever et al. (2017), so we only give a short overview here. SMASH makes use of the DECam calibrated data produced by the NOAO Community Pipeline (CP; Valdes et al. 2014)[33] which performs

[33] http://www.noao.edu/noao/staff/fvaldes/CPDocPrelim/PL201_3.html

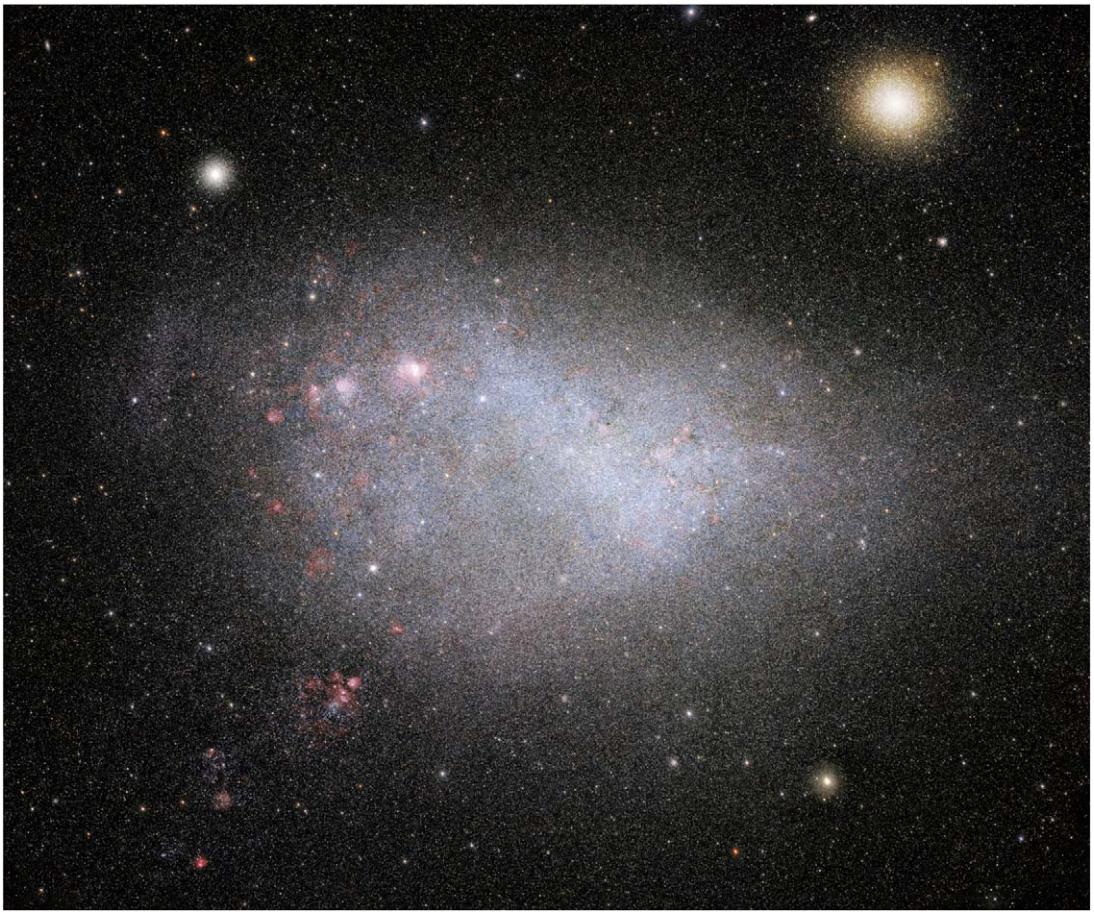

Figure 3. A three-color image of the SMASH fields in the main body of the Small Magellanic Cloud. Credit: CTIO/NOIRLab/NSF/AURA.

Table 1
SMASH Fields Table

Number	Name	RAJ2000 (hms)	DEJ2000 (hms)	RADEG (deg)	DEDEG (deg)	L_{MS}[a] (deg)	B_{MS}[a] (deg)
1	0010-6947	00:10:19.87	−69:47:40.56	2.58282	−69.794600	−19.56937	−13.84173
2	0018-7705	00:18:57.90	−77:05:00.23	4.74128	−77.083400	−12.11547	−15.01799
3	0023-7358	00:23:19.08	−73:58:08.04	5.82950	−73.968900	−15.14808	−13.94466
4	0024-7223	00:24:56.64	−72:23:08.15	6.23604	−72.385600	−16.67737	−13.38564
5	0044-7137	00:44:06.76	−71:37:45.84	11.02820	−71.629400	−16.91433	−11.74021
6	0044-7313	00:44:32.54	−73:13:31.79	11.13560	−73.225500	−15.38135	−12.28828
7	0045-7448	00:45:03.28	−74:48:14.76	11.26370	−74.804100	−13.85882	−12.82186
8	0050-8228	00:50:34.51	−82:28:26.40	12.64380	−82.474000	−6.36406	−15.28088
9	0101-7043	01:01:27.40	−70:43:05.51	15.36420	−70.718200	−17.19874	−10.09455
10	0103-7218	01:03:36.31	−72:18:54.36	15.90130	−72.315100	−15.66017	−10.63165

Note.
[a] Magellanic Stream coordinates defined in Nidever et al. (2008).

(This table is available in its entirety in machine-readable form.)

the instrument signature removal (e.g., bias subtraction, flat-fielding, etc.). The PHOTRED[34] pipeline (Nidever & Dorta 2020) is then used to perform point-spread function (PSF) photometry on each individual exposure first and forced photometry on all overlapping exposures later with DAOPHOT/ALLFRAME (Stetson 1994). Finally, custom calibration software (SMASHRED;[35] Nidever et al. 2020) is used to perform an ubercal-like calibration (Padmanabhan et al. 2008) of exposures in a field to combine measurements and to calibrate the photometry.

We obtained multiple deep (∼300 s) and shallow (60 s) exposures in every filter and a majority of our fields (with the exception of the shallow fields in the LMC). The deep exposures allow us to reach depths of 24–25th mag, while the shallow exposures fill in the brighter magnitudes (to ∼16th mag, although this is color dependent; see Figure 5). The completeness is reduced for the brightest stars, such as the tip of the red giant

[34] https://github.com/dnidever/PHOTRED
[35] https://github.com/dnidever/SMASHRED

Table 2
SMASH DECam and 0.9 m Observing Runs

Date (Nights)	Telescope	Source	Comments
		Pre-survey	
2012 Dec 11+12 (2)	4 m	Shared risk	5 pilot fields
2013 Mar 17–20 (4)	4 m	2013A-0411	23 fields (*griz*)
2013 Aug 8+9 (2 part)	4 m	Time from Saha Bulge project	Clear, 3 fields
		Survey Year 1	
2013 Sep 7–10 (4)	0.9 m	NOAO survey	Bad weather, no data
2013 Sep 11–13 (3)	0.9 m	Bought from SMARTS	Bad weather, no data
2013 Oct 21–22 (2 part)	0.9 m	Makeup for Sep 11–13	Bad weather, no data
2014 Jan 5–7 (3)	4 m	NOAO survey	0.5 night lost, 10 fields
2014 Jan 12–13 (2)	0.9 m	Makeup for Oct 21–22	2 nights photometric, 4 fields calibrated
2014 Jan 19–20 (2 half)	4 m	DD time	Clear, *riz* for 6 fields
2014 Jan 21–28 (8 half)	4 m	Chilean time	1 half night lost, 4 fields, 9 partials
2014 Jan 29–30 (2 half)	4 m	DD time	Clear, *ug* for 8 pre-survey fields
2014 Feb 13 (1 part)	4 m	Engineering	Clear, *riz* for 6 fields
2014 Feb 14–23 (10)	0.9 m	NOAO survey	9 nights photometric, 30 fields calibrated
2014 May 27–Jun 2 (7)	4 m	NOAO survey	Lost 1 night, 21 fields observed, *ug* for 13 pre-survey fields, 3 extra fields
		Survey Year 2	
2014 Sep 25–Oct 1 (7)	0.9 m	NOAO survey	1 night photometric, 11 fields calibrated
2014 Oct 11–12 (2)	4 m	Engineering	Some globular cluster calibration data
2014 Nov 21–23 (3)	4 m	NOAO survey	12 LMC/SMC main body fields
2014 Dec 17–18 (2)	4 m	NOAO survey	8 LMC/SMC main body fields
2015 Mar 13–18 (5)	4 m	NOAO survey	Mostly clear, 21 finished, 4 partials
2015 Mar 30–31 (2)	4 m	DD time	Deep & high-cadence data of Hydra II
2015 Apr 26–Mar 2 (7)	0.9 m	NOAO survey	4.5 nights photometric, 48 fields calibrated
		Survey Year 3	
2015 Oct 25–27 (2)	4 m	DD time	Bad weather, no data
2015 Nov 9 (1)	4 m	NOAO survey	Clear, 4 fields
2015 Nov 23 (1)	4 m	DD time	Bad weather, long *riz* for 2 fields
2015 Nov 27–29 (3)	0.9 m	Chilean time	9 fields calibrated
2015 Dec 5–6 (2)	4 m	NOAO survey	8 fields, 7 are LMC/SMC main body
2016 Jan 1–6 (6)	4 m	NOAO survey	4 nights lost, 3 finished, 2 partials
2016 Feb 13–18 (6)	4 m	NOAO survey	40 shallow LMC fields, 18 long fields
2016 May 8–12 (5)	4 m	NOAO survey	Bad weather, no data
		Survey Year 4—Extension	
2016 Oct 29–31 (3)	4 m	NOAO survey	0.5 night lost, 8 fields
2017 Mar 8 (0.5)	4 m	DD time	Clear, calibration data for 25 fields
2017 Aug 4 (partial)	4 m	DD time	Clear, calibration data for 3 fields
2017 Nov 29 (1)	4 m	Engineering	Clear, calibration data for 3 fields

branch, the asymptotic giant branch, and the youngest main-sequence stars. Therefore, we suggest some caution when studying these populations in the SMASH catalogs.

A substantial fraction of the SMASH fields are "island" fields that do not overlap other SMASH fields (see Figure 1). Therefore, during the standard calibration and combination steps the exposures of only one field were dealt with at a time. However, SMASH has contiguous coverage of the central regions (or main bodies) of the MCs and the fields there do overlap. Providing catalogs on a field-by-field basis would produce a large number of duplicate objects in the main bodies. To remedy this issue, an additional step was taken to combine the data uniformly in the MC main bodies. The data were combined and calibrated in a similar manner to the regular fields but using HEALPix (Górski et al. 2005) instead of fields. An `nside = 64` was used, corresponding to an area of 0.89 square degrees and resulting in 321 total HEALPix with 257/64 for LMC/SMC. The field-level ubercal zero-point corrections were used for calibrating the data in the HEALPix regions, because in some cases (HEALPix at the edges of the contiguous regions) the number of overlapping chips was too small to reliably perform the ubercal calibration. In the main body regions, both HEALPix and field-level catalogs are provided in the flat FITS files (see Section 5), but only the HEALPix catalogs are loaded in the `object` table of the database (see Section 4.1) in order to remove duplicates.

4. Description and Achieved Performance of the Final Catalogs

The SMASH DR2 data set includes 5982 DECam exposures with 359,393 separate chip files producing 4,156,198,451

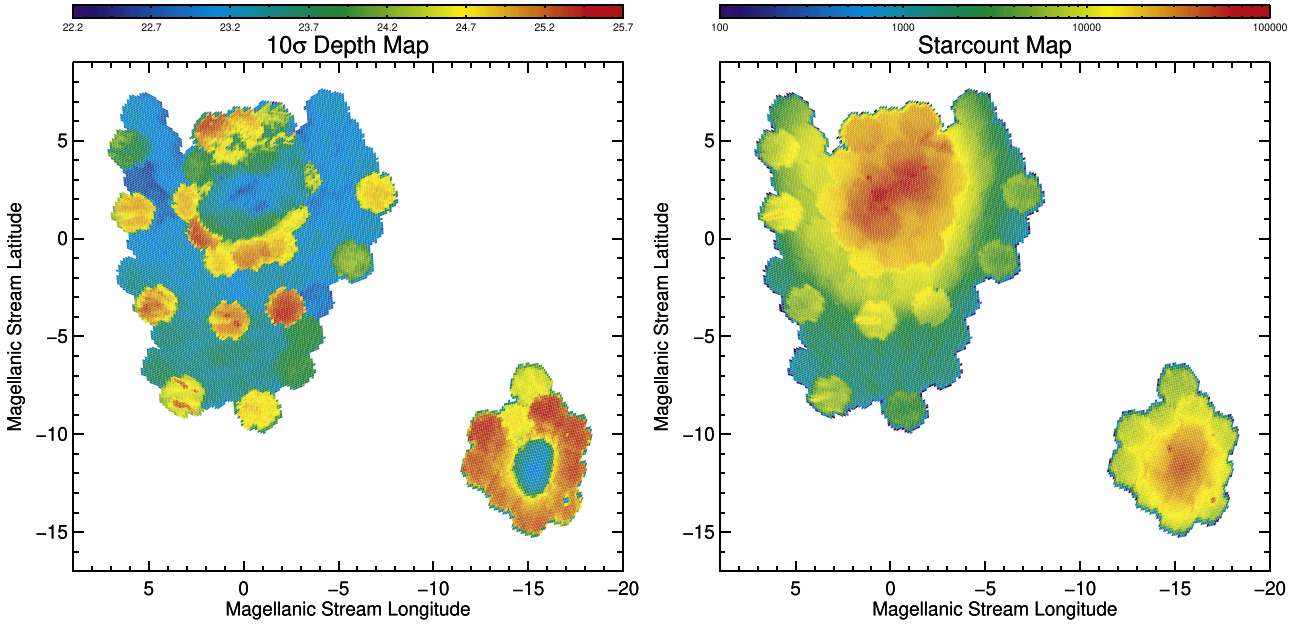

Figure 4. Left: the SMASH DR2 g-band 10σ depth in the contiguous regions in the main bodies of the MCs using nside = 512 HEALPix ($\sim 7'$ across). Right: number of objects in each HEALPix over the same region. There is reduced depth in the very crowded centers of the MCs. The 40 shallow LMC fields at somewhat larger radii can also be seen by their reduced depth.

independent source measurements of 360,363,299 unique objects.

4.1. Final Catalog Files

The final catalogs consist of eight gzip-compressed binary FITS files per field and HEALPix:

1. `FIELD/HEALPix_exposures.fits.gz`—information about each exposure;
2. `FIELD/HEALPix_chips.fits.gz`—information about each chip;
3. `FIELD/HEALPix_allsrc.fits.gz`—all of the individual source measurements for this field;
4. `FIELD/HEALPix_allobj.fits.gz`—average values for each unique object;
5. `FIELD/HEALPix_allobj_deep.fits.gz`—average values for each unique object using only the deepest exposures;
6. `FIELD/HEALPix_allobj_bright.fits.gz`—bright stars from allobj used for cross-matching between fields;
7. `FIELD/HEALPix_allobj_xmatch.fits.gz`—cross-matches between SMASH and Gaia DR2 (Gaia Collaboration et al. 2016; Brown et al. 2018), 2MASS (Skrutskie et al. 2006), and ALLWISE (Cutri et al. 2013) using catalogs from CDS VizieR;[36]
8. `FIELD/HEALPix_expmap.fits.gz`—the exposure map per band.

More detailed descriptions of the catalogs can be found in the PHOTRED `README` file on the FTP site.[37]

The photometric and astrometric performance is the same as mentioned in Nidever et al. (2017). The photometric precision (calculated using multiple independent measurements of bright stars) is 10 mmag (u), 7 mmag (g), 5 mmag (r), 8 mmag (i), and 5 mmag (z). The photometric accuracy measured from overlapping fields that are independently calibrated are 13 mmag (u), 13 mmag (g), 10 mmag (r), 12 mmag (i), and 13 mmag (z). The median 5σ point-source photometric depths in the *ugriz* bands are (23.9, 24.8, 24.5, 24.2, and 23.5) mag. Finally, the astrometric precision of individual measurements is $\sim$20 mas for bright stars, but this number increases for fainter stars with lower signal-to-noise ratio. The astrometric accuracy is $\sim$2 mas per coordinates with respect to the Gaia DR1 reference frame.

Although we used the best seeing conditions during observing runs ($\approx 1''$ in the i-band) to observe the very center of the MCs, there is still appreciable crowding in these regions that somewhat reduces the depth of the photometric catalogs. Figure 4 shows the g-band 10σ depth in the central contiguous regions of the MCs and the reduced depth due to crowding is clearly visible. These effects can also be seen in the example deep SMASH CMDs of the inner LMC and SMC in Figure 5.

5. Second Public Data Release

As mentioned above, the second SMASH public data release contains $\sim$4 billion measurements of $\sim$360 million objects in 197 fully calibrated fields covering $\sim$480 square degrees and sampling $\sim$2400 deg^2 of the Magellanic system (Figure 1). Of the 61 fields released in DR1, the data for 29 fields have been reprocessed but for the other 32 fields the catalogs are identical to those in DR1 except for some additional columns (e.g., HEALPix indices, ecliptic coordinates) that we added in DR2. As for SMASH DR1, the main data access is through the Astro Data Lab[38] hosted by NSF's National Optical-Infrared Astronomy Research Laboratory (NOIRLab). Access and exploration tools include a custom Data Discovery tool, database access to the catalog (via direct query or TAP service), an image cutout service, and

[36] https://vizier.u-strasbg.fr/viz-bin/VizieR

[37] ftp://astroarchive.noirlab.edu/public/hlsp/smash/dr2/catalogs/README.txt

[38] https://datalab.noao.edu/smash/smash.php

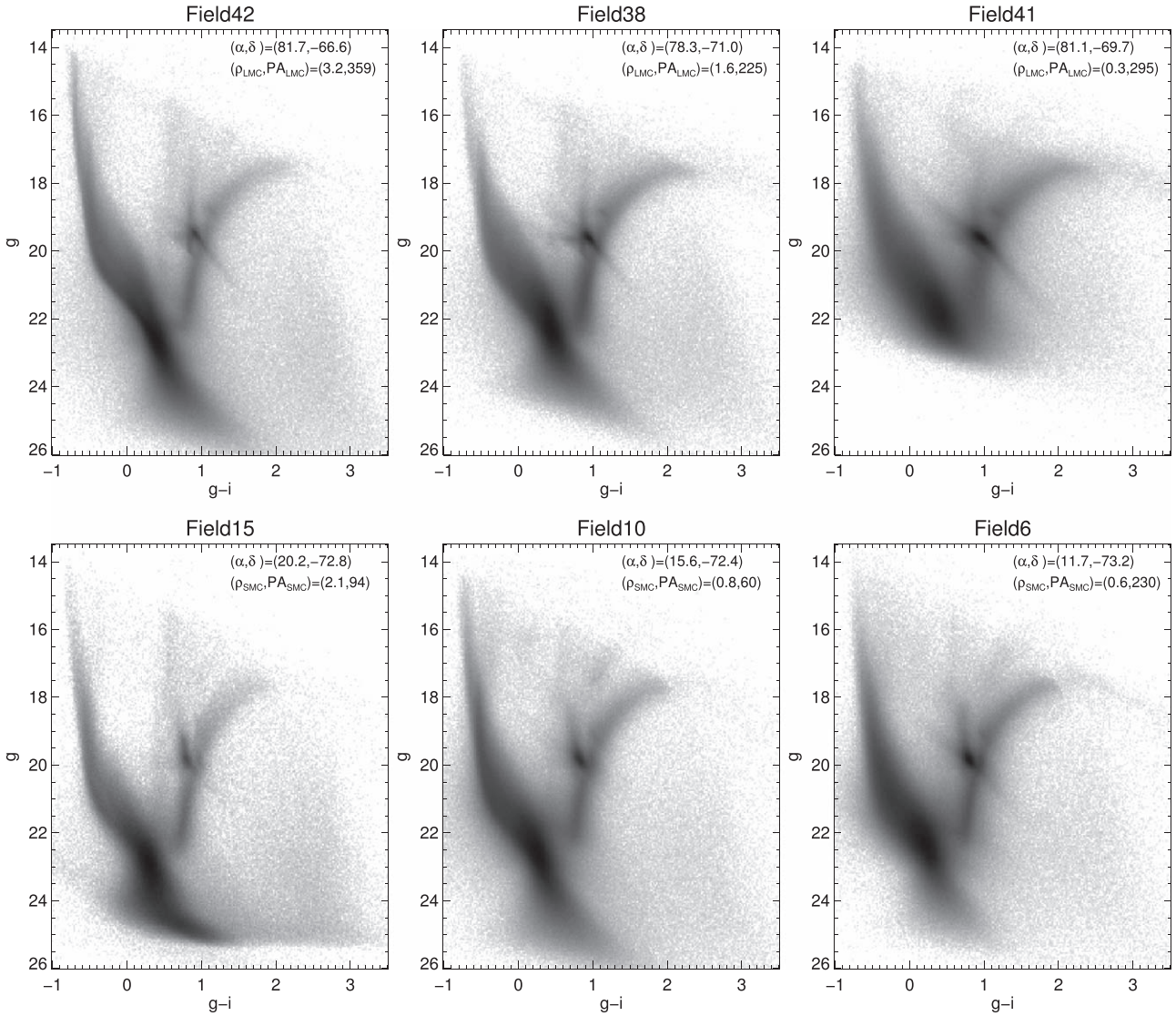

Figure 5. Example SMASH Hess diagrams of the inner LMC (top) and SMC (bottom) showing the quality of the SMASH photometry. Field42 is in the northern LMC at a radius of 3.°2 and has a significant amount of reddening. Field38 is 1.°6 from the LMC center and has somewhat reduced depth due to crowding. The center of the LMC is covered by Field41 which has substantial reddening and reduced depth. Field15 is in the eastern SMC at a radius of 2.°1 and has very young stars from the Magellanic Bridge. Field10 is 0.°8 from the SMC center and has increased reddening. Finally, Field6 covers the center of the SMC and has reduced depth due to crowding.

a Jupyter notebook server with example notebooks for exploratory analysis. The data release page also gives extensive documentation on the SMASH survey, including the observing strategy, data reduction and calibration, as well as information on the individual data products.

Images, intermediate data products, and final catalogs (in FITS binary formats) are also available through the NOIRLab High Level Data Products FTP site.[39] The raw images as well as the CP-reduced InstCal, resampled and single-band stacked images are available in `raw/`, `instcal/`, `resampled/`, and `stacked/` directories, respectively (and grouped in nightly subdirectories). Each subdirectory has a `README` file that gives information about each FITS image file (e.g., exposure number, time stamp, filter, exposure time,and field). The PHOTRED-ready FITS files and other associated files (PSF, photometry catalogs, logs, etc.) as well as the multiband stacks are available in the `photred/` directory. The final binary FITS catalogs (as described in Section 4.1) are in the `catalogs/` directory. Finally, there are seven tables in the database that were populated using the FITS catalogs (with some additional columns, e.g., HEALPix indices, ecliptic coordinates): field, exposure, chip, source, object, deep, and xmatch. The exposure map files are not loaded into the database. A detailed description of the database schema (tables and columns) is available on the Astro Data Lab website in the Query Interface.[40]

6. Science Examples

SMASH is a deep photometric survey of the MCs with the goal of understanding the low density stellar structures in the periphery as well as the complex evolution and star formation history of the inner populations. SMASH DR2 data are the

[39] ftp://astroarchive.noirlab.edu/public/hlsp/smash/dr2/

[40] https://datalab.noao.edu/query.php

deepest and most extensive covering the central regions of the MCs in a contiguous way (see Figures 2 and 3) to date and will be extremely valuable for understanding the structure and evolution of the hearts of these nearby galaxies.

6.1. Star Formation Histories

The quality and spatial coverage of the SMASH DR2 data allow us to recover deep CMDs reaching the oMSTO for the main bodies of the MCs (see Figure 5 as well as Figure 1, and Figures 11 and 12 from Nidever et al. 2017). This enables, among many other aspects, the derivation of spatially resolved star formation histories in the central LMC/SMC fields (Ruiz-Lara et al. 2020; P. Massana et al. 2021, in preparation). As an example of the reliability of SMASH data to recover SFHs, and partly as a sanity check, Figure 6 compares published SFHs with that obtained using SMASH data from the same region. For this comparison we have chosen field 11 from Monteagudo et al. (2018), located on the LMC's northwest arm (ElYoussoufi et al. 2019) within SMASH field 37. Monteagudo et al. (2018) used the VIsible Multi-Object Spectrograph (VIMOS) on the Very Large Telescope (VLT) to obtain deep *B*- and *R*-band images in several fields within the central part of the LMC. The observations were carried out under exceptional seeing conditions (seeing $\sim$0.″6–0.″8) and exposure times of 1832 s for the *B*-band and 2232 s for the *R*-band, resulting in completeness levels of $\sim$40% in the oMSTO region (compared to the nearly 80% completeness we have in SMASH field 37). The quality of the VIMOS data, the similar methodology with respect to our SMASH approach, and the compatibility of their results with SFHs from deeper HST data (see Figure 3 in Monteagudo et al. 2018) make this comparison a perfect exercise to test the reliability of SFHs recovered from SMASH data.

The methodology applied to recover SFHs from SMASH data is the result of the experience acquired over the years of members of the SMASH collaboration (e.g., Gallart et al. 1999; Harris & Zaritsky 2001; Aparicio & Gallart 2004; Monelli et al. 2010; Hidalgo et al. 2011; Monachesi et al. 2012; Meschin et al. 2014; Noël et al. 2015; Bernard et al. 2018) and it is based on the well-tested and established technique of CMD fitting (e.g., Gallart et al. 2005; Tolstoy et al. 2009; Cignoni & Tosi 2010). The basis of that method is extensively explained in Monelli et al. (2010) and Bernard et al. (2018; see also Ruiz-Lara et al. 2020 and T. Ruiz-Lara et al. 2021, in preparation for the particular case of SMASH). In short, we computed a synthetic CMD containing around 150 million stars using the BaSTI stellar evolution library (Pietrinferni et al. 2004, solar-scaled; Reimers mass loss parameter, $\eta = 0.2$; Kroupa initial mass function, Kroupa 2001; binary fraction, $\beta = 50\%$; minimum mass ratio for binaries, $q = 0.1$). This synthetic CMD is divided, following a grid in age and metallicity, in different single stellar populations (SSPs) that will be compared to the observed CMDs. Such comparison is carried out by counting the number of stars in small boxes in specific regions (bundles) within the CMD using the code `THESTORM` (Bernard et al. 2018). Prior to the comparison itself, the observational errors affecting SMASH data are simulated in the synthetic CMD. For that, we have developed a pipeline (`FAKERED`) to compute artificial star tests for the SMASH data. The routines of this pipeline were first outlined in Choi et al. (2018b). `FAKERED` first injects artificial stars of a large range of colors into the images, then reruns `PHOTRED`, and finally tabulates

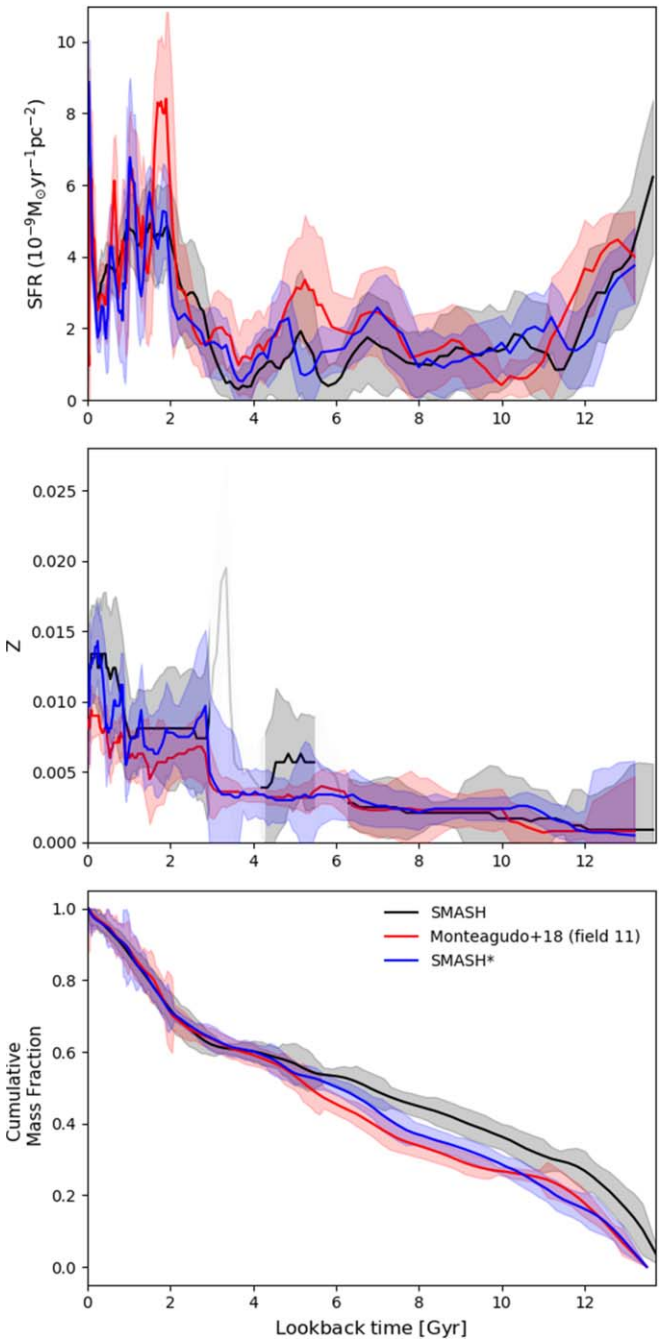

Figure 6. Comparison between the star formation histories computed using SMASH and VIMOS (Monteagudo et al. 2018) data. We show the star formation rate as a function of time (top), the chemical enrichment (middle), and the cumulative mass fraction (bottom). We compare three different solutions: SMASH (black) using SMASH data and the set of parameters that better suits the data, Monteagudo+18 (field 11, red), and SMASH* (blue) using SMASH data and mimicking the input parameters used in Monteagudo et al. (2018). The middle panel shows with transparency the age range where a small fraction of stars has been found and thus, where a fully reliable metallicity determination is hindered. Shaded regions represent uncertainties in the SFH recovery computed as described in Hidalgo et al. (2011).

which artificial stars were recovered, together with their measured magnitudes. Details about our artificial tests will be presented in T. Ruiz-Lara et al. (2021, in preparation) along with the full SFHs in the deep fields observed in the LMC. The catalog of artificial stars and the completeness maps will be released in the final SMASH data release and a more detailed

description of FAKERED will be given in the accompanying paper.

For comparison between the observed CMDs and the synthetic CMDs, we transformed the observed CMDs into the absolute plane on a star-by-star basis by taking into account spatially varying differential reddening and the distance to each field (due to the LMC's inclined disk) using the RC-based results by Choi et al. (2018b) for the LMC and Y. Choi et al. (2021, in preparation) for the SMC, respectively. Further details about deriving the SFHs using the SMASH data are given in Ruiz-Lara et al. (2020) and will be presented in future SMASH papers. All the above-described ingredients (computation of synthetic CMDs, bundle strategy, and definition of SSPs) have been carefully chosen after extensive tests to properly deal with the SMASH data.

The outcome of this methodology applied to the above-described test region is shown in Figure 6 from the analysis of SMASH (black) and VIMOS (red; Monteagudo et al. 2018) data. Although both data sets have been analyzed following the same methodology, there are slight differences regarding the bundle definition, age and metallicity bins, and synthetic CMD computation that might affect the comparison. In order to isolate the effect of the different sets of data (SMASH versus VIMOS), and thus, assessing the consistency of the SFHs derived with SMASH data with previous published determinations, we decided to run a different test (SMASH*, in blue) mimicking all the input parameters used in Monteagudo et al. (2018). In all cases the results are in agreement within uncertainties both in the star formation rate as a function of time (SFR(t); top panel) as well as in the chemical enrichment (middle panel). The main discrepancies are found at intermediate and old ages, although, even there, wiggles in the recovered SFR(t) showing maxima at ∼5, and 7 Gyr, as well as the increased SFR at ages older than ∼11 Gyr are quite coincident among the different solutions. As expected, the small differences found between SMASH and Monteagudo et al. (2018) are somewhat minimized when comparing with this second attempt, SMASH* (especially recognizable in the cumulative mass fraction panel, bottom panel of Figure 6).

At this point, we should emphasize that SMASH data not only provide SFH results that are compatible with data collected from other ground-based facilities. The VIMOS SFHs derived in Monteagudo et al. (2018) have also been contrasted, successfully, to SFHs derived using deeper HST data (see their Figure 3). We find, in agreement with previous studies of the SFH of the LMC disk (e.g., Harris & Zaritsky 2009; Meschin et al. 2014), three clearly distinct epochs: (i) an initial phase forming metal-poor, old stars (older than 11 Gyr), (ii) an epoch with lower but non-negligible star formation (3.5–11 Gyr), and (iii) a re-ignition of the star formation in the last 3.5 Gyr.

In the near future, we plan to fully exploit this splendid SMASH data set by deriving spatially resolved census of the inner region of both MCs to tackle specific science questions for which the knowledge of SFHs is essential. The first of such works has already been published (Ruiz-Lara et al. 2020), showing compelling evidence suggesting the stability and longevity of the LMC spiral arm, in place for at least ∼2 Gyr.

6.2. Star Cluster Search

The star clusters of the MCs are a valuable resource, acting as testbeds and calibrators for stellar evolution models (e.g., Marigo et al. 2008), as well as providing long-lived tracers of chemical evolution and star formation (e.g., Carrera et al. 2008; Piatti & Geisler 2013). In the LMC, the cluster age distribution is well known to feature a large number of clusters with ages less than ∼3 Gyr as well as a number of ancient globular clusters, but almost no clusters with ages between these extremes (Mateo et al. 1986; Olszewski et al. 1996). Conversely, the field shows star formation continuing throughout this epoch, albeit at a suppressed rate (Holtzman et al. 1999; Olsen 1999). The uniform, multiband SMASH observations of the main bodies of the LMC and SMC provide the necessary depth and image quality (1.″1 average seeing) to enhance star cluster searches and catalogs, and to provide a basis for comparing cluster and field star formation histories from the same data.

Previous star cluster searches and catalogs are the result of either heterogeneous data that is the combination of many individual studies spanning decades (Bica et al. 2008, 2020) or poorer data from MCPS (Hill & Zaritsky 2006; Werchan & Zaritsky 2011) or OGLE (Pietrzynski et al. 1999). The SMASH data set provides the opportunity to rederive a star cluster catalog for the MCs using uniform data and cluster detection techniques which should be more spatially complete than previous searches. This new effort aims to overcome shortcomings of recent algorithmic detection efforts (see Bitsakis et al. 2017, 2018; Piatti 2018a, 2018b) by conducting a well-characterized crowdsourced visual search of the SMASH imaging. This technique continues the long tradition of visual cluster identification across the Local Group, and builds on the legacy of crowdsourced cluster identification in the Andromeda galaxy (Johnson et al. 2015), which demonstrated the capability and robustness of this methodology.

The crowdsourced search of the SMASH data is currently underway via the Local Group Cluster Search,[41] a citizen science project hosted on the Zooniverse[42] platform. In addition to producing a uniformly derived catalog, this effort will also produce the first robust star cluster catalog completeness determination for the MC cluster population through its use of synthetic cluster tests included in the imaging. The ability to model observational completeness for the cluster sample will significantly improve population level analyses.

Beyond the updated cluster catalog, the SMASH photometric data provide deep cluster CMDs that suffer from less crowding than previous galaxy-wide photometric catalogs, enabling significant improvements to cluster CMD fitting (e.g., Glatt et al. 2010) that extend to old cluster ages. In Figure 7 we demonstrate the improvement of SMASH cluster CMDs over previous MCPS-based data. Together, the catalog and CMD improvements from SMASH will usher in a new wave of population-wide analyses of MC clusters.

6.3. Photometric Metallicities

The SMASH u-band can be used to obtain photometric metallicities by adopting the methods used by Ivezic et al. (2008) for SDSS data and Ibata et al. (2017) for the Canada–France Imaging Survey u-band together with SDSS and Pan-STARRS g, i, and r photometry. Here we introduce our analysis of SMASH dwarf stars and focus on the Magellanic MSTO population, but we also plan to investigate measuring

[41] clustersearch.org
[42] zooniverse.org

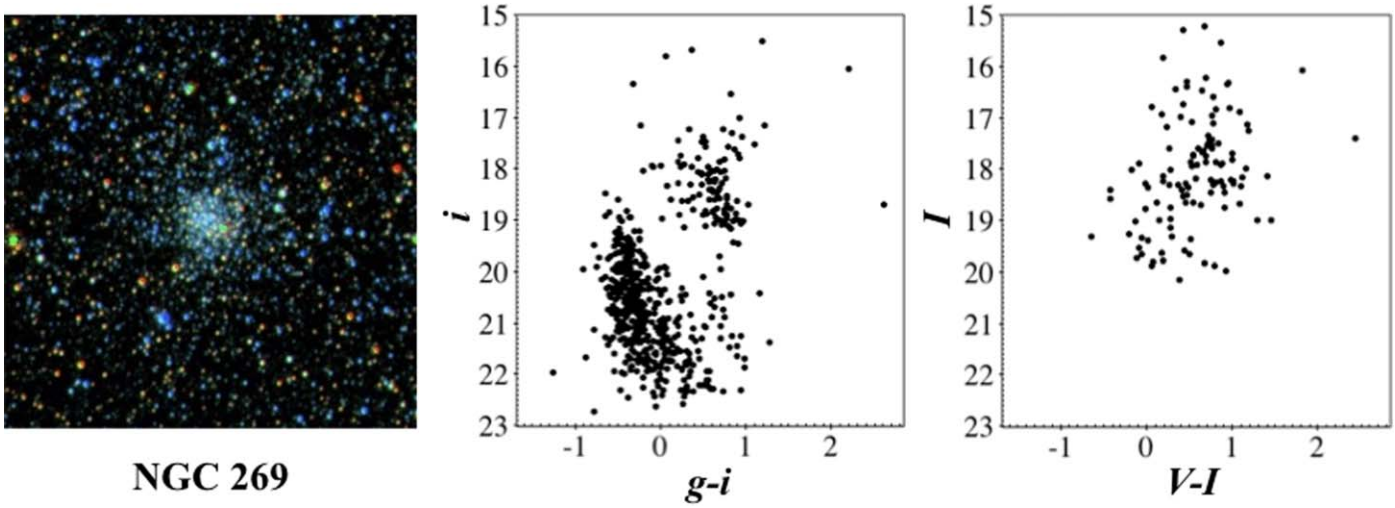

Figure 7. Cluster NGC 269 in the SMC. Left: SMASH *gri* color image, middle: SMASH CMD, and right: MCPS CMD.

metallicities for Gaia DR2 proper-motion-selected Magellanic RGB stars. We recalibrate their methods with SMASH u, g, and r photometry and two spectroscopic surveys: SDSS (Ahn et al. 2014) and the Large sky Area Multi-Object Spectroscopic Telescope (LAMOST; Luo et al. 2015). There are ∼4000 stars in SMASH standard star fields that have SDSS or LAMOST spectroscopic metallicities. We select ∼3000 dwarfs using a spectroscopic classification of $3 < \log g < 5$. We find sorting our calibration stars by $u - g$ color versus $g - r$ color is optimal for tracing metallicity of SMASH dwarf stars; this trend is supported by the literature for similar MW dwarf stars (Ivezic et al. 2008; Ibata et al. 2017). The binned calibration sample of the dwarfs with both spectroscopic metallicities and SMASH photometry is shown in the top panel of Figure 8. We also construct a set of PARSEC isochrones (Bressan et al. 2012; Marigo et al. 2017) of age 3 Gyr with a minimum and maximum metallicity value matching those of our calibration sample; the binned isochrone tracks are shown in the bottom panel of Figure 8. We use two different techniques to calculate a star's photometric metallicity with its SMASH $(u - g)_0$ and $(g - r)_0$ colors: (1) the mean of the five nearest metallicity points in the spectroscopic mean metallicity map (top panel of Figure 8), and (2) the mean of the five nearest metallicity points in the PARSEC isochrone mean metallicity map (bottom panel of Figure 8). These two methods produce very similar metallicity results.

We test our photometric metallicity technique on two prominent Milky Way clusters in our SMASH data: 47 Tucanae and NGC 362. 47 Tuc is contained within SMASH field 4 while NGC 362 is contained within SMASH field 9. Figure 9 shows the stellar density and CMD (with selected main-sequence stars in red) of 47 Tuc. We run the main-sequence populations of both clusters through our method. We obtain a metallicity of $[\mathrm{Fe/H}] = -0.76$ for 47 Tuc which is consistent with the literature value of $[\mathrm{Fe/H}] = -0.76$ (Harris 1997). For NGC 362, we obtain $[\mathrm{Fe/H}] = -1.03$ which is slightly discrepant from the literature value of $[\mathrm{Fe/H}] = -1.16$ (Harris 1997). As an additional check, we have used the high-resolution spectrosopic APOGEE-2 data from SDSS DR16 (Ahumada et al. 2020)—which targeted both of these clusters—to measure median metallicities of $[\mathrm{Fe/H}] = -0.73$ for 47 Tuc and $[\mathrm{Fe/H}] = -1.09$ for NGC 362. These results indicate that our SMASH photometric metallicities are

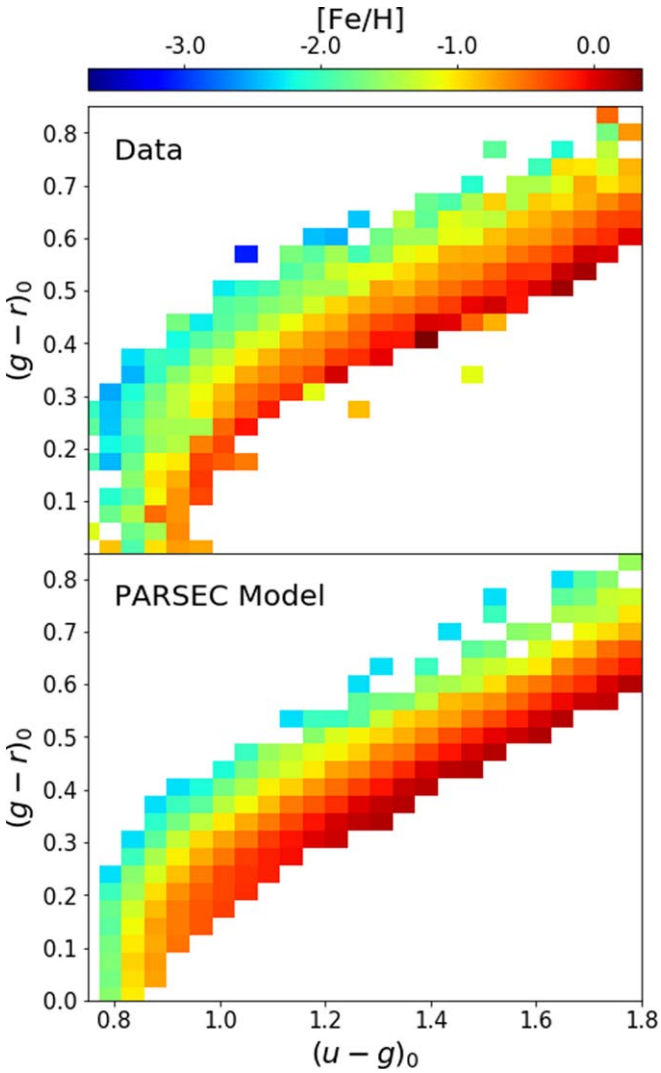

Figure 8. The SMASH MSTO range in color–color space. Top: binned SDSS and LAMOST spectroscopic median metallicity as a function of $(g - r)_0$ vs. $(u - g)_0$ in SMASH colors, with bin sizes of 0.033 dex in $(g - r)_0$ and 0.043 dex in $(u - g)_0$. Bottom: binned PARSEC isochrone metallicity with the same binning.

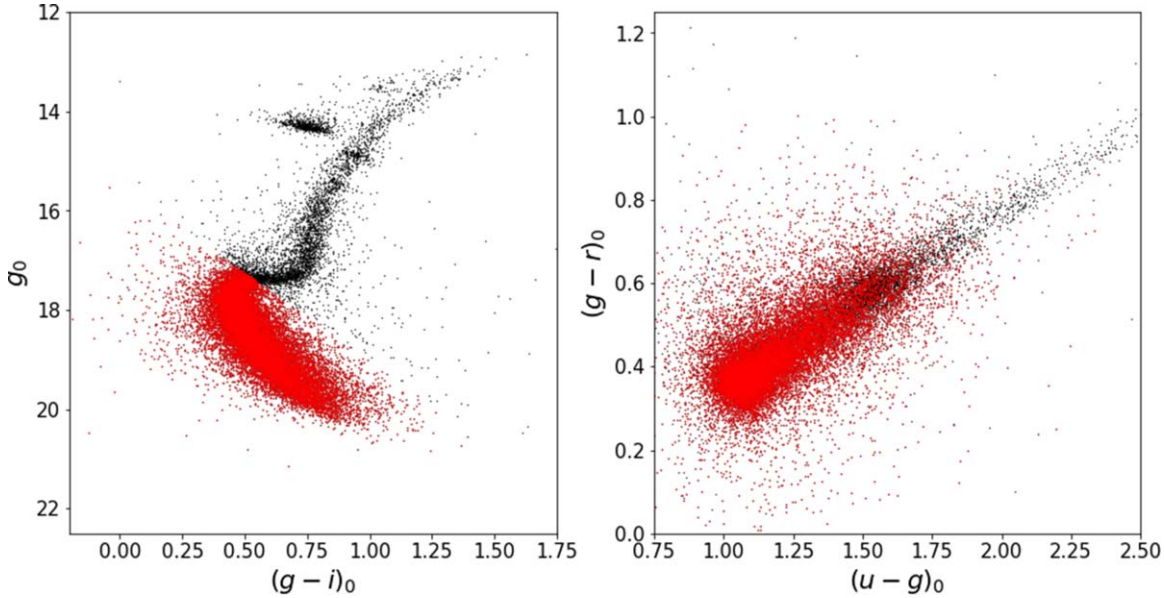

Figure 9. The MW cluster 47 Tucanae in the SMASH data. Left: CMD of the cluster member stars with the selected main-sequence population in red. Right: color–color diagram of cluster member stars.

accurate at the 0.02–0.06 dex level at metallicities of [Fe/H] ≈ -1.

Although these results demonstrate the veracity of our general technique, we acknowledge that it is more challenging to apply our method to the Magellanic MSTO populations. These stars are several magnitudes fainter than the cluster main-sequence stars and have larger photometric uncertainties. In addition, reddening can be an important issue for the *u*-band which is vital to our study. To combat these issues, we only study SMASH fields on the outer main bodies of the MCs and the Magellanic periphery where dust extinction is dominated by the MW and Schlegel et al. (1998) dust corrections can be reliably applied. Also, we will take advantage of the thousands of MSTO stars per field and use statistically robust methods to represent the average photometric metallicity. The results will be presented in an upcoming paper (A. Miller et al. 2021, in preparation) which will also investigate the effects of age and binarity on the photometric metallicities.

SMASH photometric metallicities that we measure in the Magellanic periphery will ultimately help shed light on the origin of the outer, low surface-brightness structure of the MCs (e.g., Belokurov & Erkal 2019; Nidever et al. 2019). A classical halo of accreted satellites should be quite metal-poor ([Fe/H] ≈ -2) as the satellites of the MCs would be quite low-mass and metal-poor. An in situ or puffed-up disk origin would be relatively more metal-rich and similar to the outer disk of the LMC and spheroidal component of the SMC ([Fe/H] ≈ -1). A more in-depth discussion of our photometric metallicity technique as well as the metallicity results in the outskirts of the MCs will be presented in A. Miller et al. (2021, in preparation).

7. Summary and Future Outlook

Except for the artificial star catalogs, SMASH DR2 marks the completion of the survey's public data releases, but multiple science investigations introduced in Section 6 and beyond will continue. The SMASH survey has the potential to revolutionize our understanding of the stellar populations inside and to the very outskirts of two canonical examples of dwarf galaxies, the SMC and LMC.

DECam surveys continue to explore the MCs and their surroundings, extending the investigations begun by SMASH. Of particular note, the legacy of the SMASH survey is continued as part of the DECam Local Volume Exploration (DELVE)[43] survey. This three-year, three-component NOIRLab observing program includes an MC periphery survey (DELVE-MC) that uses DECam to obtain contiguous *gri* coverage across 1000 deg^2 to a *g*-band depth of $\sim$24.2 mag.

Y.C., E.F.B., and A.M. acknowledge support from NSF grant AST 1655677. A.D., C.G., T.R.L., and M.M. acknowledge support by the Spanish Ministry of Economy and Competitiveness (MINECO) under the grants AYA2014-56795-P and AYA2017-89076-P as well as AYA2016-77237-C3-1-P. T.R.L. has support from a Spinoza grant (NWO) awarded to A. Helmi and acknowledges support by an MCIU Juan de la Cierva—Formación grant (FJCI-2016-30342). C.P.M.B. and M.-R.L.C. acknowledge support from the European Research Council (ERC) under the European Union's Horizon 2020 research and innovation program (grant agreement No. 682115). A.M. acknowledges support from FONDECYT Regular 1181797. R. R.M. acknowledges partial support from project BASAL AFB-170002 as well as FONDECYT project No. 1170364. D.M.D. acknowledges financial support from the State Agency for Research of the Spanish MCIU through the "Center of Excellence Severo Ochoa" award to the Instituto de Astrofísica de Andalucía (SEV-2017-0709). Image processing: Travis Rector (University of Alaska Anchorage), Mahdi Zamani, and Davide de Martin. We thank the anonymous referee for useful comments that improved the manuscript.

Based on observations at Cerro Tololo Inter-American Observatory, NSF's National Optical-Infrared Astronomy Research Laboratory (NOAO Prop. ID: 2013A-0411 and 2013B-0440; PI: D. L. Nidever), which is operated by the Association of Universities for Research in Astronomy (AURA)

[43] https://delve-survey.github.io/

under a cooperative agreement with the National Science Foundation. IRAF is distributed by the National Optical Astronomy Observatory, which is operated by the Association of Universities for Research in Astronomy (AURA) under a cooperative agreement with the National Science Foundation. This project used data obtained with the Dark Energy Camera (DECam), which was constructed by the Dark Energy Survey (DES) collaboration. Funding for the DES Projects has been provided by the U.S. Department of Energy, the U.S. National Science Foundation, the Ministry of Science and Education of Spain, the Science and Technology Facilities Council of the United Kingdom, the Higher Education Funding Council for England, the National Center for Supercomputing Applications at the University of Illinois at Urbana-Champaign, the Kavli Institute of Cosmological Physics at the University of Chicago, Center for Cosmology and Astro-Particle Physics at the Ohio State University, the Mitchell Institute for Fundamental Physics and Astronomy at Texas A&M University, Financiadora de Estudos e Projetos, Fundação Carlos Chagas Filho de Amparo, Financiadora de Estudos e Projetos, Fundação Carlos Chagas Filho de Amparo à Pesquisa do Estado do Rio de Janeiro, Conselho Nacional de Desenvolvimento Científico e Tecnológico and the Ministério da Ciência, Tecnologia e Inovação, the Deutsche Forschungsgemeinschaft, and the Collaborating Institutions in the Dark Energy Survey. The Collaborating Institutions are Argonne National Laboratory, the University of California at Santa Cruz, the University of Cambridge, Centro de Investigaciones Enérgeticas, Medioambientales y Tecnológicas-Madrid, the University of Chicago, University College London, the DES-Brazil Consortium, the University of Edinburgh, the Eidgenössische Technische Hochschule (ETH) Zürich, Fermi National Accelerator Laboratory, the University of Illinois at Urbana-Champaign, the Institut de Ciències de l'Espai (IEEC/CSIC), the Institut de Física d'Altes Energies, Lawrence Berkeley National Laboratory, the Ludwig-Maximilians Universität München and the associated Excellence Cluster Universe, the University of Michigan, the National Optical Astronomy Observatory, the University of Nottingham, the Ohio State University, the University of Pennsylvania, the University of Portsmouth, SLAC National Accelerator Laboratory, Stanford University, the University of Sussex, and Texas A&M University.

This work has made use of data from the European Space Agency (ESA) mission Gaia (https://www.cosmos.esa.int/gaia), processed by the Gaia Data Processing and Analysis Consortium (DPAC, https://www.cosmos.esa.int/web/gaia/dpac/consortium). Funding for the DPAC has been provided by national institutions, in particular the institutions participating in the Gaia Multilateral Agreement.

This publication makes use of data products from the Two Micron All Sky Survey, which is a joint project of the University of Massachusetts and the Infrared Processing and Analysis Center/California Institute of Technology, funded by the National Aeronautics and Space Administration and the National Science Foundation.

ORCID iDs

David L. Nidever https://orcid.org/0000-0002-1793-3689
Knut Olsen https://orcid.org/0000-0002-7134-8296
Yumi Choi https://orcid.org/0000-0003-1680-1884
Tomas Ruiz-Lara https://orcid.org/0000-0001-6984-4795
L. Clifton Johnson https://orcid.org/0000-0001-6421-0953
Cameron P. M. Bell https://orcid.org/0000-0003-0642-6558
Robert D. Blum https://orcid.org/0000-0002-8622-4237
Maria-Rosa L. Cioni https://orcid.org/0000-0002-6797-696X
Carme Gallart https://orcid.org/0000-0001-6728-806X
Steven R. Majewski https://orcid.org/0000-0003-2025-3147
Nicolas F. Martin https://orcid.org/0000-0002-1349-202X
Pol Massana https://orcid.org/0000-0002-8093-7471
Antonela Monachesi https://orcid.org/0000-0003-2325-9616
Noelia E. D. Noël https://orcid.org/0000-0002-8282-469X
Joanna D. Sakowska https://orcid.org/0000-0002-1594-1466
Roeland P. van der Marel https://orcid.org/0000-0001-7827-7825
Alistair R. Walker https://orcid.org/0000-0002-7123-8943
Dennis Zaritsky https://orcid.org/0000-0002-5177-727X
Eric F. Bell https://orcid.org/0000-0002-5564-9873
Blair C. Conn https://orcid.org/0000-0001-6959-4546
Thomas J. L. de Boer https://orcid.org/0000-0001-5486-2747
Robert A. Gruendl https://orcid.org/0000-0002-4588-6517
Matteo Monelli https://orcid.org/0000-0001-5292-6380
Ricardo R. Muñoz https://orcid.org/0000-0002-0810-5558
Abhijit Saha https://orcid.org/0000-0002-6839-4881
A. Katherina Vivas https://orcid.org/0000-0003-4341-6172
Edouard Bernard https://orcid.org/0000-0002-8722-225X
Gurtina Besla https://orcid.org/0000-0003-0715-2173
Julio A. Carballo-Bello https://orcid.org/0000-0002-3690-105X
David Martinez-Delgado https://orcid.org/0000-0003-3835-2231
Vadim Rusakov https://orcid.org/0000-0001-7633-3985
Guy S. Stringfellow https://orcid.org/0000-0003-1479-3059

References

Ahn, C. P., Alexandroff, R., Allende Prieto, C., et al. 2014, ApJS, 211, 17
Ahumada, R., Allende Prieto, C., Almeida, A., et al. 2020, ApJS, 249, 3
Aparicio, A., & Gallart, C. 2004, AJ, 128, 1465
Bell, C. P. M., Cioni, M.-R. L., Wright, A. H., et al. 2019, MNRAS, 489, 3200
Bell, C. P. M., Cioni, M.-R. L., Wright, A. H., et al. 2020, MNRAS, 499, 993
Belokurov, V. A., & Erkal, D. 2019, MNRAS, 482, L9
Bernard, E. J., Schultheis, M., di Matteo, P., et al. 2018, MNRAS, 477, 3507
Bertelli, G., Mateo, M., Chiosi, C., & Bressan, A. 1992, ApJ, 388, 400
Besla, G., Kallivayalil, N., Hernquist, L., et al. 2007, ApJ, 668, 949
Besla, G., Kallivayalil, N., Hernquist, L., et al. 2012, MNRAS, 421, 2109
Besla, G., Patton, D. R., Stierwalt, S., et al. 2018, MNRAS, 480, 3376
Bica, E., Bonatto, C., Dutra, C. M., & Santos, J. F. C. 2008, MNRAS, 389, 678
Bica, E., Westera, P., Kerber, L. D. O., et al. 2020, AJ, 159, 82
Bitsakis, T., Bonfini, P., González-López lira, R. A., et al. 2017, ApJ, 845, 56
Bitsakis, T., González-López lira, R. A., Bonfini, P., et al. 2018, ApJ, 853, 104
Bothun, G. D., & Thompson, I. B. 1988, AJ, 96, 877
Bressan, A., Marigo, P., Girardi, L., et al. 2012, MNRAS, 427, 127
Brocato, E., Castellani, V., Ferraro, F. R., Piersimoni, A. M., & Testa, V. 1996, MNRAS, 282, 614
Brown, A. G. A., Vallenari, A., Prusti, T., & de Bruijne, J. H. J. 2018, A&A, 616, A1
Carrera, R., Gallart, C., Hardy, E., Aparicio, A., & Zinn, R. 2008, AJ, 135, 836
Choi, Y., Nidever, D. L., Olsen, K., et al. 2018a, ApJ, 869, 125
Choi, Y., Nidever, D. L., Olsen, K., et al. 2018b, ApJ, 866, 90
Cignoni, M., Cole, A. A., Tosi, M., et al. 2013, ApJ, 775, 83
Cignoni, M., & Tosi, M. 2010, AdAst, 2010, 158568
Cioni, M. R. L., Clementini, G., Girardi, L., et al. 2011, A&A, 527, A116
Cutri, R. M., Wright, E. L., Conrow, T., et al. 2013, yCat, 2328, 0
Dark Energy Survey Collaboration, Abbott, T., Abdalla, F. B., et al. 2016, MNRAS, 460, 1270

de Vaucouleurs, G. 1955a, AJ, 60, 126
de Vaucouleurs, G. 1955b, AJ, 60, 219
Elson, R. A. W., Gilmore, G. F., & Santiago, B. X. 1997, MNRAS, 289, 157
ElYoussoufi, D., Cioni, M.-R. L., Bell, C. P. M., et al. 2019, MNRAS, 490, 1076
Erkal, D., Belokurov, V., Laporte, C. F. P., et al. 2019, MNRAS, 487, 2685
Flaugher, B., Diehl, H. T., Honscheid, K., et al. 2015, AJ, 150, 150
Frogel, J. A., & Blanco, V. M. 1983, ApJL, 274, L57
Gaia Collaboration, Prusti, T., de Bruijne, J. H. J., et al. 2016, A&A, 595, A1
Gallart, C., Freedman, W. L., Aparicio, A., Bertelli, G., & Chiosi, C. 1999, AJ, 118, 2245
Gallart, C., Stetson, P. B., Hardy, E., Pont, F., & Zinn, R. 2004, ApJL, 614, L109
Gallart, C., Stetson, P. B., Meschin, I. P., Pont, F., & Hardy, E. 2008, ApJL, 682, L89
Gallart, C., Zoccali, M., & Aparicio, A. 2005, ARA&A, 43, 387
Gardiner, L. T., & Hatzidimitriou, D. 1992, MNRAS, 257, 195
Gatto, M., Ripepi, V., Bellazzini, M., et al. 2020, MNRAS, 499, 4114
Glatt, K., Grebel, E. K., & Koch, A. 2010, A&A, 517, A50
Górski, K. M., Hivon, E., Banday, A. J., et al. 2005, ApJ, 622, 759
Hardy, E., Buonanno, R., Corsi, C. E., Janes, K. A., & Schommer, R. A. 1984, ApJ, 278, 592
Harris, J., & Zaritsky, D. 2001, ApJS, 136, 25
Harris, J., & Zaritsky, D. 2004, AJ, 127, 1531
Harris, J., & Zaritsky, D. 2009, AJ, 138, 1243
Harris, W. E. 1997, yCat, 7202, 0
Hidalgo, S. L., Aparicio, A., Skillman, E., et al. 2011, ApJ, 730, 14
Hill, A., & Zaritsky, D. 2006, AJ, 131, 414
Hodge, P. 1987, PASP, 99, 730
Holtzman, J. A., Gallagher, J. S. I., Cole, A. A., et al. 1999, AJ, 118, 2262
Ibata, R. A., McConnachie, A., Cuillandre, J.-C., et al. 2017, ApJ, 848, 129
Irwin, M. J. 1991, in IAU Symp. 148, The Magellanic Clouds, ed. R. Haynes & D. Milne (Dordrecht: Kluwer), 453
Ivezic, Z., Sesar, B., Juric, M., et al. 2008, ApJ, 684, 40
Johnson, L. C., Seth, A. C., Dalcanton, J. J., et al. 2015, ApJ, 802, 127
Kallivayalil, N., van der Marel, R. P., Alcock, C., et al. 2006, ApJ, 638, 772
Kallivayalil, N., van der Marel, R. P., Besla, G., Anderson, J., & Alcock, C. 2013, ApJ, 764, 161
Kroupa, P. 2001, MNRAS, 322, 231
Luo, A.-L., Zhao, Y.-H., Zhao, G., et al. 2015, RAA, 15, 1095
Majewski, S. R., Nidever, D. L., Muñoz, R. R., et al. 2009, in IAU Symp. 256, The Magellanic System: Stars, Gas, and Galaxies, ed. J. T. Van Loon & J. M. Oliveira (Cambridge: Cambridge Univ. Press), 51
Marigo, P., Girardi, L., Bressan, A., et al. 2008, A&A, 482, 883
Marigo, P., Girardi, L., Bressan, A., et al. 2017, ApJ, 835, 77
Martin, N. F., Jungbluth, V., Nidever, D. L., et al. 2016, ApJL, 830, L10
Martin, N. F., Nidever, D. L., Besla, G., et al. 2015, ApJL, 804, L5
Martínez-Delgado, D., Katherina Vivas, A., Grebel, E. K., et al. 2019, A&A, 631, A98
Massana, P., Noël, N. E. D., Nidever, D. L., et al. 2020, MNRAS, 498, 1034
Mateo, M., Hodge, P., & Schommer, R. A. 1986, ApJ, 311, 113
Mau, S., Cerny, W., Pace, A. B., et al. 2020, ApJ, 890, 136
Meschin, I., Gallart, C., Aparicio, A., et al. 2014, MNRAS, 438, 1067
Monachesi, A., Trager, S. C., Lauer, T. R., et al. 2012, ApJ, 745, 97
Monelli, M., Hidalgo, S. L., Stetson, P. B., et al. 2010, ApJ, 720, 1225
Monteagudo, L., Gallart, C., Monelli, M., Bernard, E. J., & Stetson, P. B. 2018, MNRAS, 473, L16
Nidever, D., & Dorta, A. 2020, dnidever/PHOTRED: SMASH DR2 Release, version v1.1.0, Zenodo, doi:10.5281/ZENODO.4291682
Nidever, D., Olsen, K., Choi, Y. & SMASH Team 2020, dnidever/SMASHRED: SMASH DR2, version v1.0.0, Zenodo, doi:10.5281/ZENODO.4291646
Nidever, D. L., Majewski, S. R., & Butler Burton, W. 2008, ApJ, 679, 432
Nidever, D. L., Majewski, S. R., Butler Burton, W., & Nigra, L. 2010, ApJ, 723, 1618
Nidever, D. L., Majewski, S. R., Muñoz, R. R., et al. 2011, ApJL, 733, L10
Nidever, D. L., Olsen, K., Choi, Y., et al. 2019, ApJ, 874, 118
Nidever, D. L., Olsen, K., Walker, A. R., et al. 2017, AJ, 154, 199
Noël, N. E. D., Conn, B. C., Read, J. I., et al. 2015, MNRAS, 452, 4222
Noël, N. E. D., & Gallart, C. 2007, ApJL, 665, L23
Olsen, K. A. G. 1999, AJ, 117, 2244
Olszewski, E. W., Suntzeff, N. B., & Mateo, M. 1996, ARA&A, 34, 511
Padmanabhan, N., Schlegel, D. J., Finkbeiner, D. P., et al. 2008, ApJ, 674, 1217
Piatti, A. E. 2018a, MNRAS, 475, 2553
Piatti, A. E. 2018b, MNRAS, 478, 784
Piatti, A. E., & Geisler, D. 2013, AJ, 145, 17
Pietrinferni, A., Cassisi, S., Salaris, M., & Castelli, F. 2004, ApJ, 612, 168
Pietrzynski, G., Udalski, A., Kubiak, M., et al. 1999, AcA, 49, 521
Rest, A., Stubbs, C., Becker, A. C., et al. 2005, ApJ, 634, 1103
Ripepi, V., Cignoni, M., Tosi, M., et al. 2014, MNRAS, 442, 1897
Rubele, S., Pastorelli, G., Girardi, L., et al. 2018, MNRAS, 478, 5017
Ruiz-Lara, T., Gallart, C., Monelli, M., et al. 2020, A&A, 639, L3
Saha, A., Olszewski, E. W., Brondel, B., et al. 2010, AJ, 140, 1719
Schlegel, D. J., Finkbeiner, D. P., & Davis, M. 1998, ApJ, 500, 525
Skrutskie, M. F., Cutri, R. M., Stiening, R., et al. 2006, AJ, 131, 1163
Smecker-Hane, T. A., Cole, A. A., Gallagher, J. S. I., & Stetson, P. B. 2002, ApJ, 566, 239
Stetson, P. B. 1994, PASP, 106, 250
Stryker, L. L. 1984, ApJS, 55, 127
Tolstoy, E., Hill, V., & Tosi, M. 2009, ARA&A, 47, 371
Torrealba, G., Belokurov, V., Koposov, S. E., et al. 2018, MNRAS, 475, 5085
Udalski, A., Szymanski, M., Kaluzny, J., Kubiak, M., & Mateo, M. 1992, AcA, 42, 253
Valdes, F., Gruendl, R. & DES Project 2014, in ASP Conf. Ser. 485, The DECam Community Pipeline, ed. N. Manset & P. Forshay (San Francisco, CA: ASP), 379
Vivas, A. K., Olsen, K., Blum, R., et al. 2016, AJ, 151, 118
Weisz, D. R., Dolphin, A. E., Skillman, E. D., et al. 2013, MNRAS, 431, 364
Werchan, F., & Zaritsky, D. 2011, AJ, 142, 48
Westerlund, B. E. 1970, VA, 12, 335
Zaritsky, D., Harris, J., Thompson, I. B., Grebel, E. K., & Massey, P. 2002, AJ, 123, 855